Mohammad Reza Bagheri
Hamid Mehdigholi
Mohammad Said Seif
Omar Yaakob
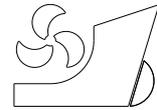
AN EXPERIMENTAL AND NUMERICAL PREDICTION OF MARINE PROPELLER NOISE UNDER CAVITATING AND NON-CAVITATING CONDITIONS

Summary

In this study, the hydrodynamics and noise prediction of a five blade marine propeller were analyzed through numerical and experimental methods under variety operational conditions. The hydrodynamics of the propeller was studied and the characteristic curves were presented in both numerical and experimental methods. Inception and development of sheet cavitation conditions are obtained in both numerical and experimental methods. The cavitation was started and developed by either increasing the propeller rotational speed in constant pressure or decreasing pressure, while the velocity was kept constant. Good agreements are observed between numerical and experimental results, qualitatively and quantitatively. The noise of the propeller was analyzed through Computational fluid dynamics (CFD) method, based on the formulation of Ffowcs Williams and Hawkings (FW-H). Similarly, the experimental results collected from hydrophones were compared with numerical simulations. Finally, the effects of reflection in cavitation tunnel were obtained by considering overall sound pressure levels in numerical and experimental results.

Key words: *CFD; FW-H; Cavitation tunnel; Propeller hydrodynamics; Propeller noise*

1. Introduction

Three major sources of underwater noise, produced by underwater and surface vehicles, are the machinery, propeller and the flow noise. There are four mechanisms to produce the pressure waves by the propeller [1, 2]. The cavitation noise is the major source of noise of the propeller, it should be thoroughly investigated. The low frequency noise is a result of sheet cavitation on the surfaces of the blades [2].

The experimental works of the cavitation noise have been represented for various purposes, including detecting the inception and development of sheet cavitation and predicting cavitating and non-cavitating noise levels [3]. The propeller noise measurement is

cost-effective in the water tank or free water for each full-scale. Therefore, the noise measurement of model propeller is performed using the cavitation tunnel. The net propeller noise measurements for different operating conditions in the cavitation tunnel were reported by the 18th ITTC cavitation committee (1987) [4, 5]. UKON et al., in 1987, studied the acoustic field measurement in a cavitation tunnel [6]. BARK, in 1987, investigated cavitation noise from Sydney Express propeller [7]. ZHU et al., in 1978, studied the effects of wall reflections [8]. Sharma et al., in 1990, investigated some marine propellers in cavitation tunnel [9]. Atlar et al., in 2001, investigated cavitation tunnel tests for propeller noise of a Fisheries Research Vessel (FRV) which their research was carried out in Emerson Cavitation Tunnel (ECT) [10]. In a later research, Wang et al., in 2006, studied an experimental investigation on cavitation and noise characteristics of ocean stream turbines in the ECT [11]. Emin et.al, in 2012, studied an experimental study into the effect of foul release coating on the efficiency, noise and cavitation characteristics of a propeller [12]. Park et al., in 2009, studied noise source localization in a cavitation tunnel [3]. As mentioned, many experimental researches have been conducted to measure the propeller noise in the cavitation tunnel. The effects of wall reflections are important in the cavitation tunnel tests. A common way for evaluating wall reflections is to measure the propeller noise both in the cavitation tunnel and free water tests. The difference of the Sound Pressure Levels (SPLs) obtained from these tests is considered as the effects of wall reflections in the cavitation tunnel. Examples of such studies were reported by 18th ITTC cavitation committee [4]. In order to extract propeller net noise; many researches were performed by numerical simulations using FW-H equations.

Seol et al., in 2002 and 2005, presented a study on the non-cavitating and cavitating underwater propeller noise [13, 14]. They described the use of a hybrid method to predict the underwater propeller noise. Their results were presented in one operative condition and in the low frequency range. Caro et al., in 2007, presented a Computational Aero-Acoustics (CAA) formulation based on Lighthill analogy for fan noise using CFD method [15]. Jin-Ming et al., in 2012, investigated the noise of a three-blade propeller and they concluded that the overall spectrum of sound in front of the propeller hub, for same distance, is more than the propeller rotating plane [16]. Ianniello et al., in 2013, investigated noise nonlinear analysis a marine propeller base on FW-H equations [17]. PAN et al., in 2013, evaluated marine propeller noise in non-uniform flow by FW-H equation [18].

In the experimental part of this study, the hydrodynamics and noise of marine propeller are investigated in a cavitation tunnel. The effects of pressure drop and propeller rotational speed incensement are studied on the cavitation inception and extent. Also, the effect of cavitation extent was studied on the overall noise of propeller. The aim of the numerical section is to obtain the acoustic field and hydrodynamic analysis of a marine propeller in the uniform inflow. Moreover, the various parameters such as: input velocity, propeller rotational speed, and etc., are investigated to extract the conditions of the cavitation inception and were used in the experimental tests. Also, all the propeller operational curves were optimized using grid study. The flow analysis results are used as the noise source in the equations for obtaining the overall SPLs. Therefore, the results from hydrodynamics analysis are compared to and verified against the experimental findings from the cavitation tunnel. In the present study, the sheet cavitation effect on increasing the overall SPLs is investigated as the most important sound source for cavitation in low frequencies.

2. Methodology of flow and acoustic analysis

The basic equation for sound propagation is the Lighthill equation obtained from the continuity and momentum equations [19]. The FW-H is a solution developed from the

An Experimental and Numerical Prediction of Marine
Propeller Noise under Cavitating and Non-Cavitating
Mohammad Reza Bagheri, Hamid Mehdigholi
Mohammad Said Seif, etc.

Lighthill equation. In present work, the FW-H formulation is used to extract overall SPLs in the far field by CFD method. The FW-H formulation is represented by Equation (1) [20].

$$\frac{1}{c_0^2}\frac{\partial^2 p'}{\partial t^2} - \nabla^2 p' = \frac{\partial^2}{\partial x_i x_j}\left[T_{ij}H(f)\right] - \frac{\partial}{\partial x_i}\left(\left[P_{ij}n_j + \rho u_i(u_n - v_n)\right]\delta(f)\right) +$$

$$\frac{\partial}{\partial t}\left(\rho_0 v_n + \rho(u_n - v_n)\right)\delta(f) \tag{1}$$

The terms in the right side of Equation (1) are called quadruple, dipole and monopole sources, respectively. p' is the sound pressure at the far-field. Setting $f{=}0$ introduces a surface that embeds the external flow effect ($f{>}0$), while c_0 is the far-field sound speed and T_{ij} is the Lighthill stress tensor. $H(f)$ and $\delta(f)$ are Heaviside and Dirac delta functions, respectively. Farassat proposed a formulation for solving the FW-H equation in time domain [21]. In Farassat formulation, the pressure field is defined by Equations (2) to (4).

$$p'(\vec{x},t) = p'_T(\vec{x},t) + p'_L(\vec{x},t) \tag{2}$$

$$4\pi p'_T(\vec{x},t) = \int_{f=0}\left[\frac{\rho_0 \dot{v}_n}{r(1-M_r)^2}\right]_{ret} dS + \int_{f=0}\left[\frac{\rho_0 v_n(r\dot{M}_i\hat{r}_i + c_0 M_r - c_0 M^2)}{r^2(1-M_r)^3}\right]_{ret} dS \tag{3}$$

$$4\pi p'_L(\vec{x},t) = \frac{1}{c_0}\int_{f=0}\left[\frac{\dot{l}_i\hat{r}_i}{r(1-M_r)^2}\right]_{ret} dS + \int_{f=0}\left[\frac{l_r - l_i M_i}{r^2(1-M_r)^2}\right]_{ret} dS +$$

$$\frac{1}{c_0}\int_{f=0}\left[\frac{l_r(r\dot{M}_i\hat{r}_i + c_0 M_r - c_0 M^2)}{r^2(1-M_r)^3}\right]_{ret} dS \tag{4}$$

Where p' is the acoustic pressure; p'_T and p'_L describe the acoustic pressure field resulting from thickness and loading, corresponding to the monopole and the dipole sources, e.g. blade rotation and unsteady sheet cavitation on blades are defined as monopole sources and fluctuation pressure on the blade surface is defined as a dipole source. $r = |x(t) - y(\tau)|$ is the distance between receiver and source; x and t are the sound receiver position and time, respectively. Also, y and τ are the source position and the time, respectively. M is the Mach number; $M_r = M_i\hat{r}_i$ is the component of the Mach number vector in the direction of the receiver, and $\hat{r}_i = r_i / r$ defines the unit vector in the radiation direction. l_i is the local force per unit area in direction i while l_r is equal to $l_i r_i$. v is the local normal velocity of the blade surface. $c_0 = 1500\text{m/s}$ and $\rho_0 = 1025\text{kg/m}^3$ are the sound speed and water density.

In the present study, the flow around the object is obtained to determine the source of the noise. Flow effects as blade rotation, unsteady sheet cavitation and fluctuation pressure on the blade surface are used as the input for the noise analysis. The flow field of the propeller is obtained using CFD by solution Reynolds-averaged Navier–Stokes equations (RANS equations). The FW-H acoustics model in CFD code allows you to select multiple source surfaces and receivers. In this work, the surfaces of the propeller blades are selected by

integral surfaces, *f=0*, in Equations (3) and (4). The main objective of the cavitation physical is to extract the mass fraction of vapor and liquid phases. In this study, a multi-phase method [22] is used in order to extract vapor volume fraction. Therefore, in the hydrodynamic analysis of the flow, the flow field was predicted by solving the continuity and momentum equations. The basic equation for sound propagation is the Lighthill equation which is obtained from combination between the continuity and momentum equations. The three source terms on the right-hand side of Equation (1) are the monopole, dipole and quadrupole terms which are obtained from flow field results by solving the Reynolds- Averaged Navier-Stoks (RANS). Noise prediction can be represented as the solution of the wave equation if the distribution of sources on the moving boundary (the blade surface) and in the flow field is known. Setting *f=0* in Equation (3) and (4) describes a surface that embeds the external flow (*f>0*) effect. In this research, *f=0* is the blade surfaces of propeller which obtained flow field, including velocity magnitude and pressure distribution, is considered on it as sound sources. Therefore, the flow around propeller is solved using RANS equations and then flow data are used as the input for FW-H equation to predict the far-field acoustics.

3. Numerical Analysis, Model Geometry and Grid Generation

In this paper, a five-blade propeller model is used which has $D = 0.15$m and $A_E / A_0 = 0.7$. This model was designed at the Center of Excellence in Hydrodynamics and Dynamics of Marine Vehicles (CEHDMV) and is a research model with high application at CEHDMV. Figure 1 shows several information and quantities, such as the geometries, surface grids on the blade and hub surfaces, the computational domains of the model, and the boundary conditions. The solution of the Unsteady RANS equations for utilizing the *Re-Normalization Group* (*RNG*) $k - \varepsilon$ turbulence model and the FWH sound equation is performed by the CFD. The RNG $k - \varepsilon$ model is based on the standard $k - \varepsilon$ model but has many advantages [23].Type of the grid, size of the meshes, and quality are the main contributing factors in the accuracy of numerical simulation of any geometry, since their compositions affect the convergence/divergence of the solution to a great extent. Here, convective terms are discretized using the second order accurate upwind scheme, while the velocity-pressure coupling and the overall solution procedure are based on the Semi-Implicit Method for Pressure Linked Equations-Consistent (SIMPLEC) type. The blade surface is meshed with triangles grids, while the regions around the root, tip and blade edges are meshed with smaller triangles, i.e. with sides of approximately 0.001*D*. The remaining region in the domain is then filled with hexahedron cells.
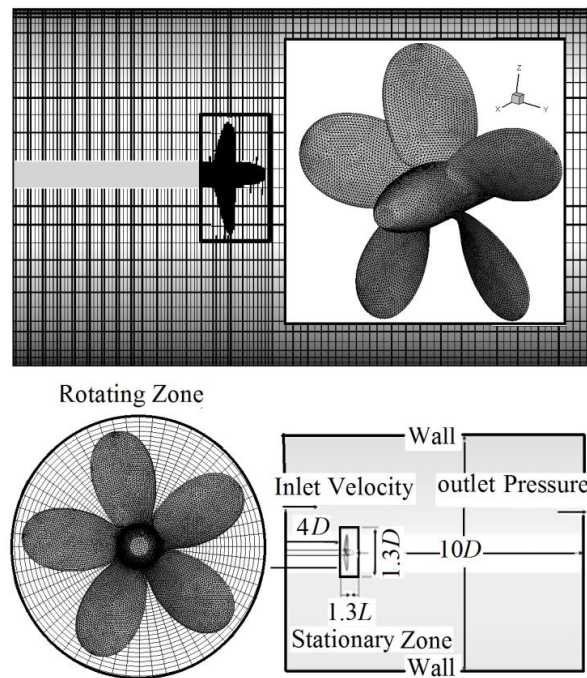
Fig. 1 Grids of model, computational domain and boundary conditions

We also considered zones, named rotating zones, which contained the flow around the propeller, and stationary zones which contained the flow around the moving zone. A cylindrical shape is assumed for the rotating zone, with a diameter of $1.3D$ and a length of $1.3L$, where L is the length of propeller hub. The rotating zone is solved via Moving Reference Frame (MRF). The inlet is situated in $4D$ distance in the upstream, while the outlet is located at $10D$ downstream and the outer boundary is at $5D$ from the shaft axis. In order to simulate the flow around the rotating propeller where the inlet boundary is located, we had imposed the velocity components for a uniform stream with a given inflow speed. At the blade and hub surface, a wall condition had imposed, while a wall boundary condition along with constant pressure conditions are imposed at the lateral and outlet boundaries, respectively.

It is important to keep the cell thickness along the body thinner than the boundary layer. The value of coefficient y^+ was the main criterion for setting the mesh resolution. The coefficient should be in a range of $30 < y^+ < 500$ [23, 24] in order to model properly the turbulent boundary layer and obtain correct pressure distributions on the propeller blade surfaces for the $k-\varepsilon$ model. The y^+ value along the propeller surface was around $+27$ to 110, see Figure 2.
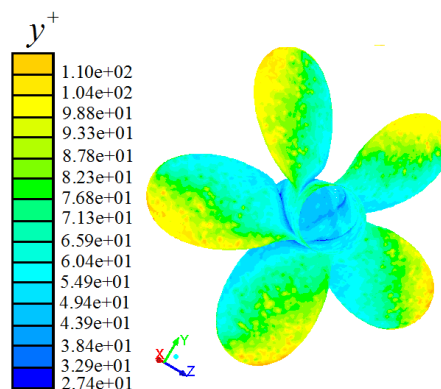
Fig. 2 Distribution of y^+ on the blade surface

At first, the number of meshes is considered 1.5 million. By this number of meshes, the vapor volume fraction was not occurred on the blade surface despite their occurrence in the experiments. Therefore, in order to observe vapor volume fraction on the blade surface, the number of cells increased from 1.5 to 3.5 million. In this condition, cavitation or vapor volume fraction happened on the blade surfaces in $J= 0.2$. In order to consider the grid independency, trust and torque coefficients were considered for addition three sets of grids, grid 1, 2 and 3 contained 1.5, 3.5 and 4 million meshes, respectively. In these sets of grids, the edge and tip of blades were mostly refined which is important in cavitation simulation of propeller. K_T and K_Q have been calculated and compared to experiment. Table 1 shows trust and torque coefficients in different grids for $J= 0.4$, 0.6 and 0.8, respectively. As seen, the total thrust and torque values increase with grid refinement from 1.5 to 3.5 grids, and tend to the experimental values. The coefficients are not changed for this model when the number of grids increased from 3.5 to 4 million meshes. Finally, the number of 3.5 million meshes selected and the results are presented for this number of meshes.

Table 1 Comparison of grid study and experiment results

	K_T	K_Q	Error K_T [%]	Error K_Q [%]
$J= 0.4$				
Experiment	0.3454	0.05298	-	-
Grid 1	0.3101	0.04905	10.22	6.53
Grid 2	0.3396	0.05174	1.67	2.34
Grid 3	0.3391	0.05168	1.82	2.45
$J= 0.6$				
Experiment	0.2495	0.04088	-	-
Grid 1	0.2203	0.03793	11.70	7.21
Grid 2	0.2359	0.03897	5.45	4.67
Grid 3	0.2348	0.03834	5.89	6.21
$J= 0.8$				
Experiment	0.1451	0.0270	-	-
Grid 1	0.1359	0.0238	6.34	11.85
Grid 2	0.1447	0.0259	1.89	4.07
Grid 3	0.1447	0.0259	1.89	4.07

4. Test setup and testing laboratory

Open water tests are carried out according to the ITTC procedure using K23 cavitation tunnel. The K23 cavitation tunnel, located at the CEHDMV in Sharif University is a recirculation tunnel with a rectangular measuring section, 2300 mm long, 650 mm wide and 350 mm deep. The cavitation tunnel test section can be seen in Figure 3.

Fig. 3 Test section K23 cavitation tunnel

To obtain the characteristic curves in the hydrodynamics tests, the propeller rotational speed is kept constant, and the flow speed is varied in the allowable range of cavitation tunnel, at 0-3.6m/s. In acoustic tests, the flow velocity is kept constant and the rotational speed is varied in the range of 300-1600 rpm to investigate the effects of increasing rotational speed on the propeller overall noise.

In the numerical study, cavitation and vapor volume fraction appearance is initiated in advance coefficient $J= 0.2$, which is corresponding to $N= 1400$ rpm and $V= 0.7$ m/s. In the experimental test, the cavitation phenomenon is exactly started in the range predicted by the numerical results. The tunnel flow speed is kept constant at 0.7 m/s during cavitation inception measurements. Two procedures are generated for cavitation development conditions in the tunnel. In the first method, the flow velocity and ambient pressure are kept at 0.7 m/s and 90 kPa, respectively and then the rotational speed of propeller is increased from 1400 rpm to 1600 rpm. In the second method, the rotational speed of propeller and flow velocity are fixed in $N=1400$ rpm and $V=0.7$ m/s, respectively and then ambient pressure in tunnel is decreased from 90 kPa to 70 kPa. A Sony alpha SLT-α 33 video camera, with an appropriate electronic shutter, used for video recording and image capturing of inception and development cavitation. The qualitative comparison between the numerical and experimental results for the cavitation inception and development is presented in the results section.

The same test setup considered for noise measurements according to the 18th ITTC cavitation committee recommendations [4]. In order to measure the propeller noise in K23 cavitation tunnel, two B&k 8103 hydrophones were used. The position of hydrophones shows in Figure 4 and Table 2. The hydrophones are well fixed in positions on Plexiglas section in the cavitation tunnel.
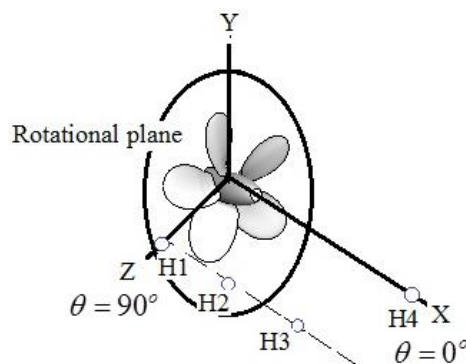
Fig. 4 Sketch of the coordinate system and Hydrophone position

Table 2 Coordinates of hydrophones and their applications in numerical and experimental method

Hydrophone	X (m)	Y (m)	Z (m)	Θ (x-z)	Numerical	Experimental
H1	0	0	0.225	90º	✓	✓
H2	0.25	0	0.225	90º	✓	-
H3	0.50	0	0.225	90º	✓	✓
H4	0.75	0	0	0º	✓	-

The following steps are carried out to extract net propeller noise:

- Measuring flow noise in tunnel when dynamometer is off.
- Measuring flow and dynamometer noise when propeller is not installed in the tunnel.
- Measuring total noise in tunnel when the propeller rotates.

For the above steps, each test is repeated tree times and the uncertainty measurements have been obtained $\pm 3dB$.

5. Results and discussions

5.1 Numerical and Experimental Results of the Hydrodynamics Analysis

In numerical simulation, the cavitation phenomenon was well investigated. Cavitation and vapor volume fraction appears in $J= 0.2$, which is equivalent to $N= 1400$ rpm and $V= 0.7$ m/s. Figure 5 presents the vapor volume fraction for two $J= 0.2$ and 0.17. Also, this figure shows the cavity growing on the blades of model. In this Figure the vapor volume fraction on the surfaces of blades dramatically increases, when the rotational speed is increased from 1400 rpm to 1600 rpm. The results of cavitation numbers, σ, at different points of the blade, S, are presented in Table 4.
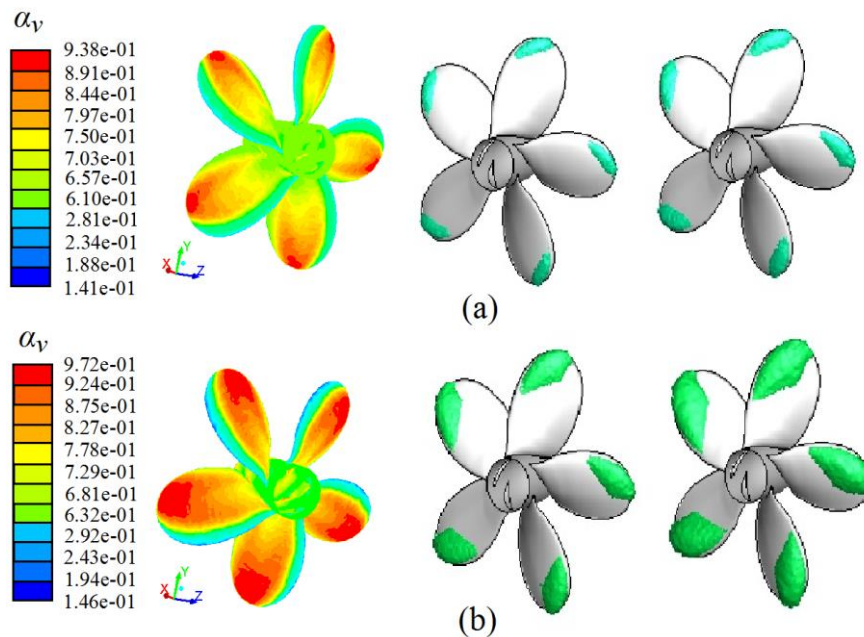
Fig. 5 The vapor volume fraction and extent of sheet cavity on the blade surfaces in numerical simulation (a) $J= 0.2$ and (b) $J= 0.17$

Table 3 Cavitation numbers in different points of blade

J	S	σ
0.20	R	0.41
	$0.7R$	1.10
0.17	R	0.24
	$0.7R$	0.95

Figure 6 presents the thrust, torque and efficiency coefficients for the various grids in numerical simulation and compared with experimental results. In Figure 6, a good agreement observes between the numerical and experimental results.
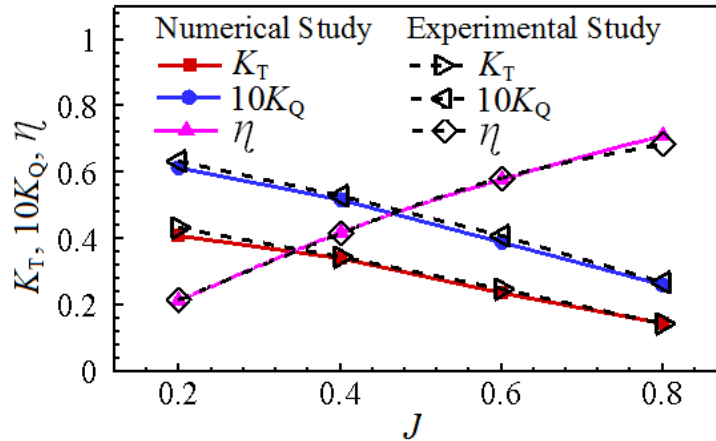
Fig. 6 Comparison of numerical simulations with experimental results for trust, torque and efficiency coefficient

The experimental investigation also indicates that cavitation phenomenon is extended by the pressure drop in the cavitation tunnel. Figure 7 shows that the cavitation inception and development were for constant rotational speed, N=1400rpm, and flow velocity, V= 0.7 m/s, for pressure drop of 70 and 90 kPa in two numerical and experimental methods. Cavitation value and vapor volume fraction on blade surface is found to increase with pressure drop in cavitation tunnel. As observed in Figure 7, sheet and tip cavitation increase in blade tip which is seen as pale halation in experimental tests while in the numerical simulation it has been marked by green color. It is observed that the cavity pattern well agrees with in the experiment tests.
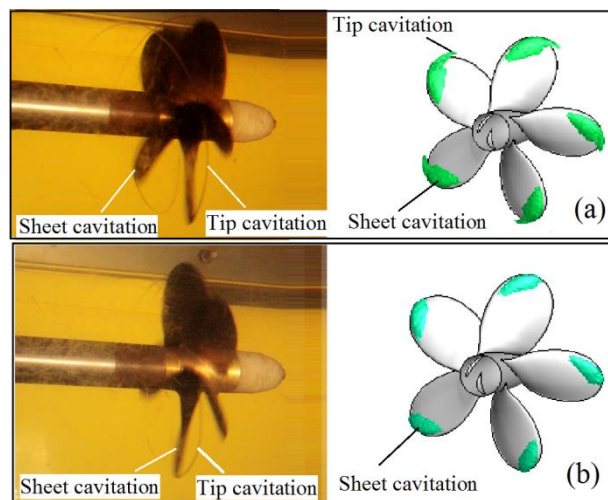
Fig. 7 Qualitative comparison of the cavitation inception and development in experimental tests together with numerical simulation (a: J=0.2 and p=70kPa, b: J=0.2 and p=90kPa)

5.2   Numerical and Experimental Results of the Acoustics Analysis

5.2.1   Noise Numerical Results

The overall SPLs are calculated using the FW-H equation and by CFD which assume infinite perimeter with no reflections. Therefore, the outcomes can be considered the propeller net noise in free-field. In order to obtain the overall SPLs at different distances from the propeller's hub for both cavitating and non-cavitating cases. Four hydrophones are used in numerical study which their positions are shown in Table 3 and Figure 3. The reference level in the solid body is considered as a source of the sound where it is the blade surfaces.

Hydrophone 1 is placed in rotation plane of propeller. Figure 8 shows the overall SPLs in hydrophone 1 for J= 0.2 and 0.3. The maximum of overall SPLs observed at the blade passing frequency (BPF), see Figure 8.
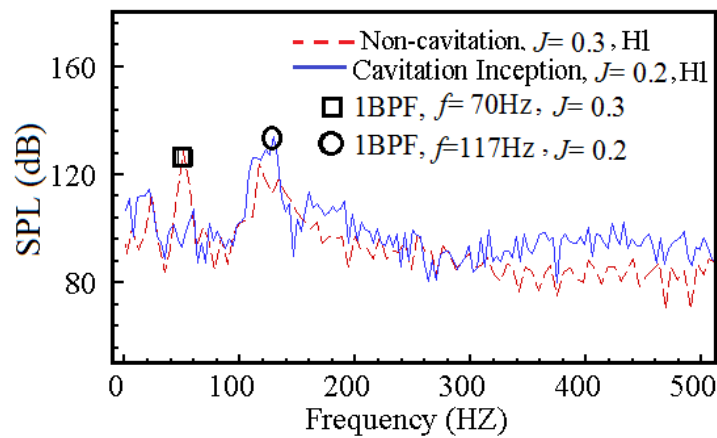
Fig. 8 The overall SPLs of H1 for J= 0.3 and 0.2

The overall SPLs under non-cavitation, cavitation inception and development conditions for hydrophones 2 to 4 are presented in Figures 9 to 11. The overall SPLs include all sound sources which are obtained from the flow solution results. As seen in Figures 9 to 11 the overall SPL reduces with increasing the distance from the sound source according to the inverse square of the distance law.
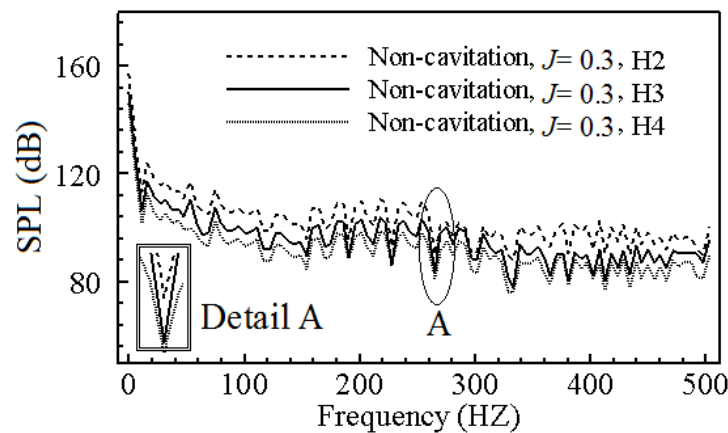
Fig. 9 The overall SPLs from numerical simulations for N=900rpm (J=0.3) and p=90kPa
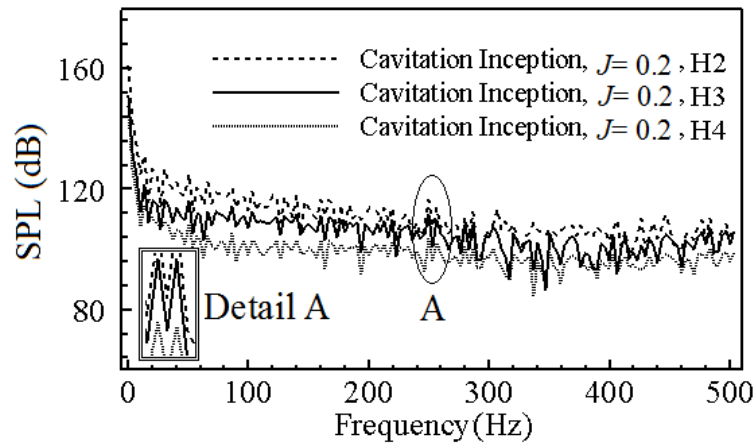
Fig. 10 The overall SPLs from numerical simulations for N=1400rpm (J=0.2) and p=90kPa
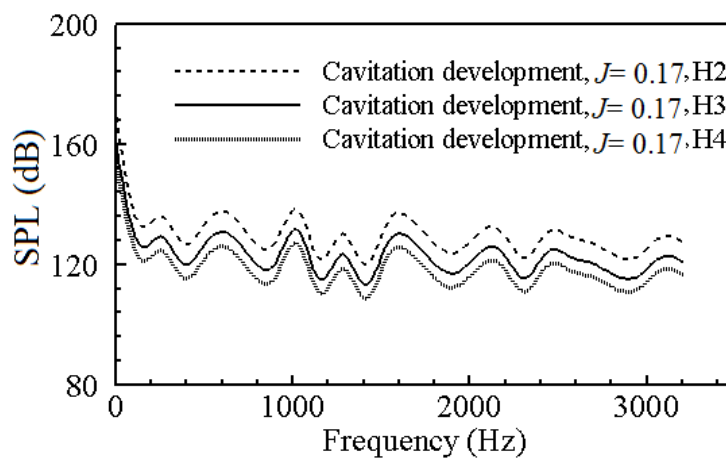
Fig. 11 The overall SPLs from numerical simulations for N=1600rpm (J=0.17) and p=90kPa

The propeller noise is proportionally increased when the rotational speed of propeller is increased; see Figures 12 to 14. These figures show comparison between overall SPLs for non-cavitating, cavitating inception and development states.
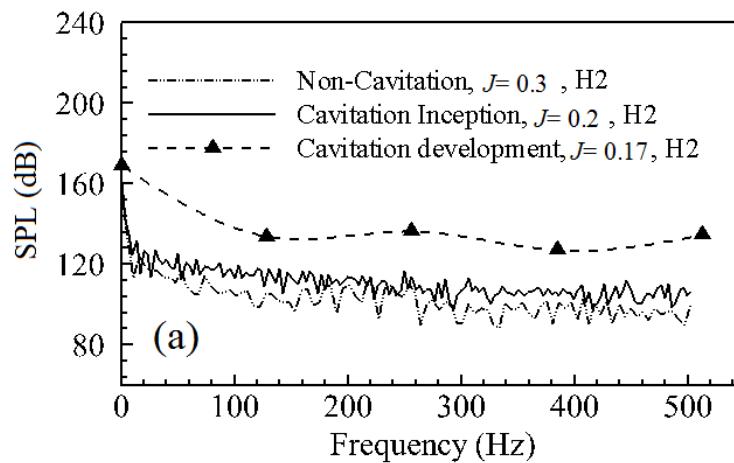
Fig. 12 The comparison of overall SPLs for H2 in J= 0.3, 0.2 and 0.17
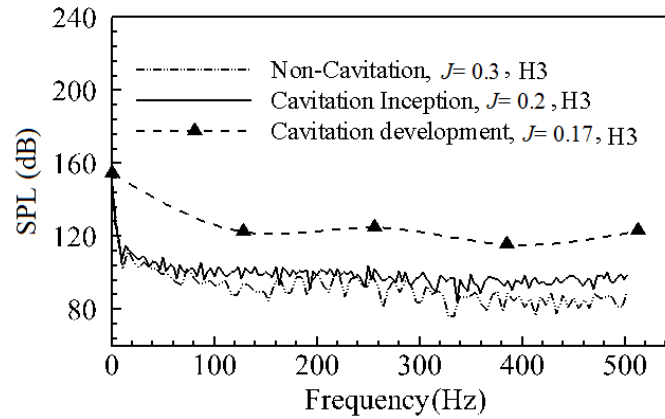
Fig. 13 The comparison of overall SPLs for H3 in *J*= 0.3, 0.2 and 0.17
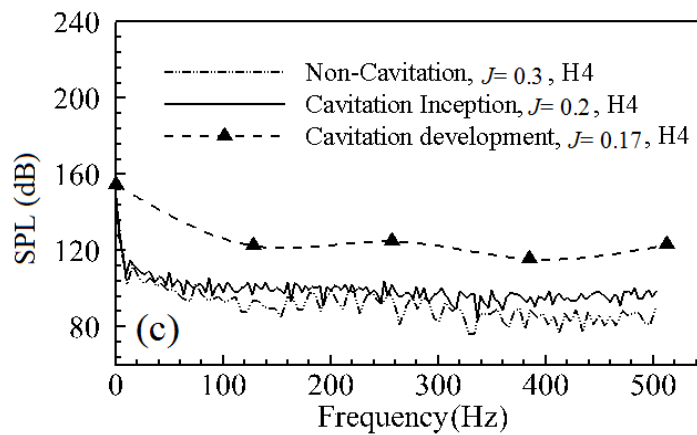
Fig. 14 The comparison of overall SPLs for H4 in *J*= 0.3, 0.2 and 0.17

The difference between overall SPL in non-cavitation and cavitation inception conditions is approximately in the range of 5 to 20 dB for each frequency. This range of difference is related to the increasing of propeller rotational speed from 900 to 1400 rpm. In comparison overall SPLs under cavitation development condition with both other conditions, the difference between the overall SPL is in the range of 10 to 30 dB. This difference depict that cavitation sheet source has much contribution in the increasing of overall SPLs in low frequency. Also, the level range is confirmed by comparing with the results in [9].

As mentioned already, the FW-H equation is solved assuming infinite field and there is not reflections from surrounding environment. Therefore, numerical results in this work can be considered as net propeller noise measurement results in free-field. As a novelty of the present work, the SPL of cavitation tunnel wall reflection has been calculated. For this purpose, it is necessary to make a discussion on the results of the experimental section which led to measuring the propeller noise in the cavitation tunnel.

5.2.2   Noise Experimental Results

The model scale measurements and procedures have been submitted to the ITTC committee and reported in the Specialist Committee on Hydrodynamic Noise for the 27th ITTC [25]. The total SPLs of the propeller at wideband are first recorded at frequencies ranging from 20 Hz to 20 kHz, which included both the total noise in tunnel (propeller noise, equipment vibration, dynamometer noise and circulation noise of flow), and the noise generated by the background noise. In order to calculate the noise generated in the tunnel, the background noise is measured separately and subtracted logarithmically from the total measured noise.

In this study, the results of net propeller noise presented in 1/3 octave band for each center frequencies [26]. The measured values of SPLs in each one-third octave band to an equivalent 1Hz bandwidth by means of the correction formula as follows [10]:

$$SPL_1 = SPL_m - 10\log \Delta f \tag{5}$$

Where, SPL_m and Δf are measured SPL at each center frequency and bandwidth for each 1/3 octave band filter in 1Hz, respectively. The net SPL (SPL_N) is calculated at each center frequency using Equation (6).

$$SPL_N = 10\log\left[10^{(SPL_T/10)} - 10^{(SPL_B/10)}\right] \tag{6}$$

Here SPL_T and SPL_B are total and background $SPLs$, respectively, measured at an equivalent 1Hz bandwidth and 1m. Time history signals are transformed to the frequency domain using Fast Fourier Transform (FFT) utility in Matlab code. Numerical method simulates only the sheet cavitation which happens on blade surfaces while in experiments, cloud cavitation and edge vortex exist in downstream and close to hydrophone 3. This effects increase the SPL in downstream region especially at hydrophone 3.

The experimental results for the SPLs for two hydrophones 1 and 3 in the constant pressure, 90 kPa, three rotational speeds N= 900, 1400, 1600 rpm and constant inlet velocity, V= 0.7 m/s, are shown in Figure 15. As seen in this Figure, the SPLs rise with the increasing in rotational speed of the propeller. Figure 16 presents the experimental results of the SPLs in two hydrophone for pressure drop from 90 to 70 kPa in J= 0.20. It is observed that SPLs gradual increase in low frequency range as pressure decreases.
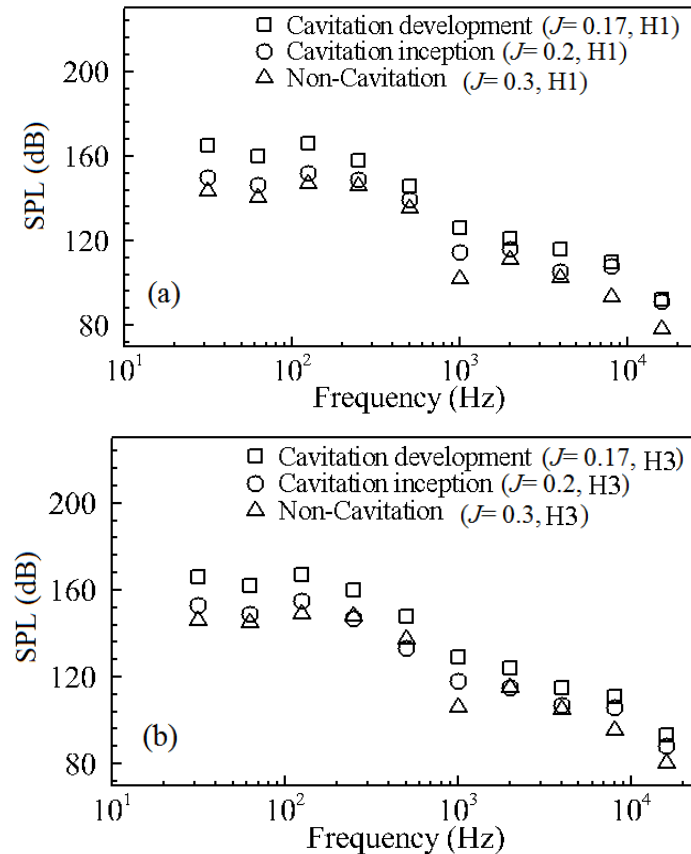
Fig. 15 Experimental SPLs of propeller in (a) H1 and (b) H3
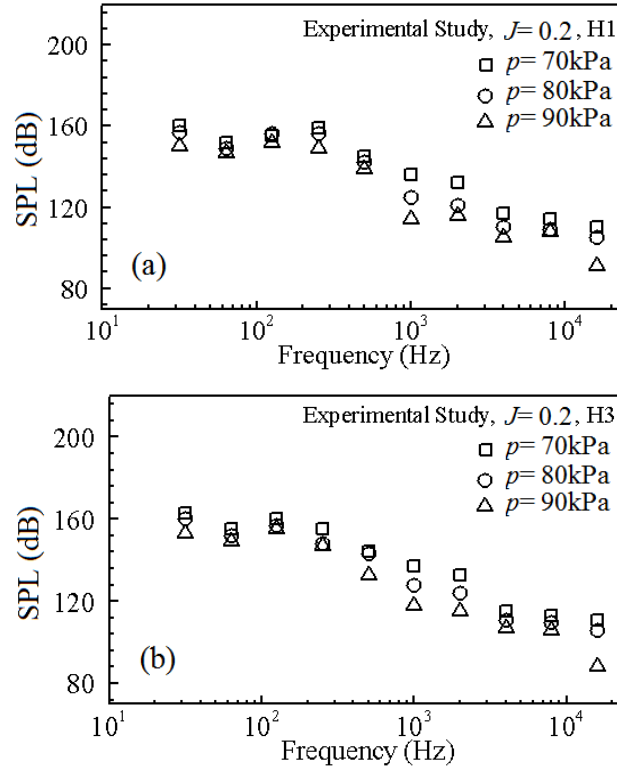
Fig. 16 SPLs of propeller in pressure drop from 90 to70kpa for J= 0.20 in (a) H1 and (b) H3

Generally, vortex cavitation and small bubbles detaching from the sheet cavitation cause increasing noise level in high frequency range. However in low frequencies, large noises are due to the increasing volumes of sheet cavitation on propeller blade surfaces which act like large vibrating bubbles. Therefore, it can be concluded that fully developed cavitation is extended at pressures under 80 kPa for J=0.2. Of course, if cavitation development conditions happened in higher rotational speeds of propeller, then fully developed cavitation is occurred at pressure upper 80 kPa. The difference of SPLs for three assumed pressures is 3-6 dB for fully developed cavitation, in frequency range lower than 500 Hz. However, it is 4-12 dB for frequency range upper than 500 Hz, see Figure 16.

The SPLs of the received signal of hydrophone 3 are larger than those of the hydrophone 1, which are mainly because the distance between the dynamometer and the hydrophone 3 is relatively short, and the non-linear effects, e.g. cloud cavitation, occur in downstream flow close to the hydrophone 3. The SPLs obtained in this study are almost in the same range and behaviour as in the previous studies for other types of propellers [10-18].

5.3   Analysis of cavitation tunnel effects

FW-H equation is used for far-field and it does not include reflection effects of computational domain. Authors assured that numerical SPLs results of this equation can be used as free-field results which have been validated in Figures 6 and 7. But cavitation tunnel is a full reverberation environment; and wall reflections affect on the net noise results of propeller. The difference of SPLs between experimental and numerical results is introduced as effect of tunnel reflections and nonlinear terms as cloud cavitation. Zhu and et al., [8] studied the measurement of tunnel wall effects by experimental method. In present work, the tunnel wall reflection coefficient, $k(f)$, has been defined by Equation (7).

$$k(f) = 20\log(\frac{P_t(f)}{P_d(f)}) \qquad (7)$$

Where $P_d(f)$ and $P_t(f)$ are Fourier transforms of $P_d(t)$ signal in free-field and $P_t(t)$ signal in cavitation tunnel, respectively. The Equation (7) can be reviewed as Equation (8).

$$k(f) = 20\log\left(\frac{\dfrac{P_t(f)}{P_{ref}(f)}}{\dfrac{P_d(f)}{P_{ref}(f)}}\right) = 20\left[\log\left(\frac{P_t(f)}{P_{ref}(f)}\right) - \log\left(\frac{P_d(f)}{P_{ref}(f)}\right)\right] =$$

$$SPL_t - SPL_d = SPL_{Experimental} - SPL_{Numerical} \tag{8}$$

According to the results in previous sections, Figures 8, 13, 15a and 15b, and using Equation (8), $k(f)$ can be calculated in each center frequency. Figure 17 depicts the results of approximation effects of cavitation tunnel reflections. It is seen that the $k(f)$ amount in low frequency range is more than that in high frequency range which is due to the higher absorptions of sound in higher frequencies for most materials. The $k(f)$ have low amount in cavitation development conditions especially in frequency range upper than 500 Hz.

Parameter $k(f)$ can be defined as appropriate approximation for the reflection effects of cavitation tunnel walls. In fact this parameter presents the overall effects in cavitation tunnel, as cloud and vortex cavitation and reflections effects of tunnel walls. This method can be applied to extract approximate effects of wall reflections when there is not appropriate equipment for noise measurements of full-scale propeller in the free-field.
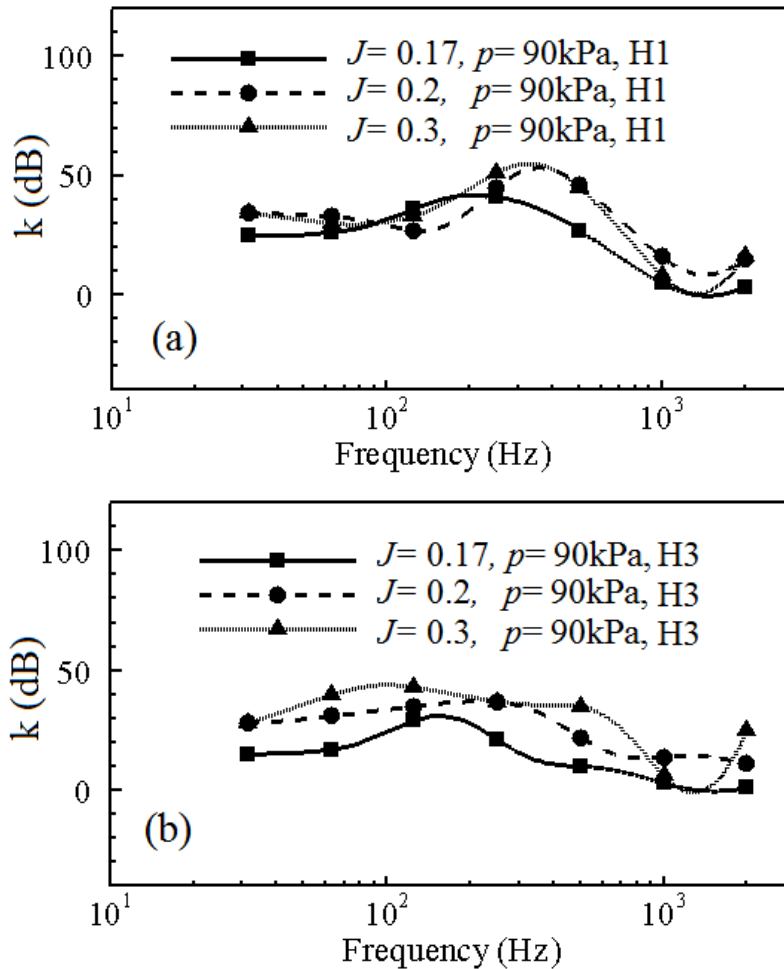
Fig. 17 The effects of cavitation tunnel in H1 and H3

6. Conclusion

In this research, a complete parametric study investigated on pressure drop and rotational speed in order to find out cavitation inception and development and their effects on the propeller noise. Cavitation inception accursed in the range of N=1200 rpm to 1400 rpm for a five blade propeller. It is found that the pressure drop in the constant rotational speed is more effective on the cavitation inception compared to the increase in the rotational speed. Fully developed cavitation is extended at pressures under 80 kPa for J=0.2. The difference of SPLs for different pressures from 90 to 70 kPa is 3-6 dB for fully developed cavitation in frequencies lower than 500 Hz, but it is 4-12 dB for frequencies upper than 500 Hz. The difference between overall SPLs in non-cavitation and cavitation inception conditions are approximately in range 5 to 20 dB in each frequency which is related to increase of propeller rotational speed from 900 to 1400 rpm. In comparison overall SPLs under cavitation development condition with two other conditions, the difference between the overall SPL is in range 10 to 30 dB.

The difference in the overall SPL, obtained from the numerical and experimental approaches, is attributed to the reflections from the effect of tunnel. Therefore, the numerical results can be used as the results for free-field. As an important contribution of this research, the tunnel cavitation effects predicted approximately. It is seen that this effects in low frequency range are more than that in high frequency range. It is suggested that these effects are introduced from difference between experimental and numerical SPLs. Of interesting results that of comparison between numerical and experimental results are observed, this subject is that with increasing rotational speed of propeller and fully cavitation development on blade surface in each frequency, reflection coefficient is decreased.

REFERENCES

[1]   D. Ross: Mechanics of underwater noise. Peninsula Publishing.CA: Los Altos, 1987.

[2]   J.S. Carlton: Marine Propellers and Propulsion. Butterworth Heinemann, London, 1994.

[3]   C. Park, H. Seol, K. Kim and W. Seong. A study on propeller noise source localization in a cavitation tunnel. J Ocean Engineering, 36: 754–762, 2009.

[4]   18th Cavitation Committee. Report of Cavitation Committee. Proc. of 18th ITTC; 1: Kobe, 1987.

[5]   H. Kato, H. Yuasa, N. Okamura: On comparative noise measurements with the 'sydney express propeller model. Proc. of 16th and 17th ITTC, 1985.

[6]   Y. Ukon, T. Kudo: Acoustic field measurement in a cavitation tunnel. Proc. of 18th ITTC; 1: Kobe, 1987.

[7]   G. Bark: Cavitation noise from Sydney express propeller model in SSPA cavitation tunnel. Proc. of 18th ITTC; 1: Kobe, 1987.

[8]   W. Zhu, H. Wang and W. Ye: Measurement of tunnel wall effect in the cavitation noise tests. 15th ITTC proceedings part I, report of cavitation committee 1978.

[9]   S.D. Sharma, K. Mani and V.H. Arakeri: Cavitation Noise Studies on marine propellers. J Sound and Vibration; 138(2): 255-283, 1990.

[10]   M. Atlar, A.C. Takinaci, E. Korkut: Cavitation tunnel tests for propeller noise of a FRV and comparisons with full-scale measurements. In: CAV Fourth International Symposium on Cavitation, California Institute of Technology ,Pasadena: CA USA , 20-23June, 2001.

[11]   D. Wang, M. Atlar, R. Sampson: An experimental investigation on cavitation, noise, and slipstream characteristics of ocean stream turbines. J. Power and Energy 2007; 221, Part A: pp. 219- 231.

[12]   E. Korkut, M. Atlar: An experimental investigation of the effect of foul release coating application on performance, noise and cavitation characteristics of marine propellers. J Ocean Engineering,; 41: 1–12, 2012.

[13]   H. Seol, B. Jung, J.C. Suh and S. Lee: Prediction of non-cavitation underwater propeller noise. J sound and vibration; 257(1): 13–157, 2002.

[14]   H. Seol, B. Jung, J.C. Suh and S. Lee: Development of hybrid method for the prediction of underwater propeller noise. J Sound and Vibration; 288: 345–360, 2005.

[15]   S. Caro, R. Sandboge, I. Iyer and Y. Nishio: Presentation of a CAA formulation based on LightHill's analogy for fan noise. Conference on fan noise; Lyon, 17-19 Sep 2007.

[16]   Y. Jin-ming, X. Ying, L. Fang and W. zhan-zhi: Numerical prediction of blade frequency noise of cavitating propeller. J Hydrodynamics; 24(3): 371-377, 2012.

[17]   R. Ianniello, R. Muscari and A. Mascio: Ship underwater noise assessment by the acoustic analogy, part III: measurements versus numerical predictions on a full-scale ship. J Marine Science and Technology 2013.DOI: 10.1007/s00773-013-0228-z.

[18]   Y.C. Pan, H.X. Zhang: Numerical prediction of marine propeller noise in non-uniform inflow. J China Ocean Eng; 27: 33-42, 2013.

[19]   M.J. Lighthill: On sound generated aerodynamically. I. General theory. Proc, R. Soc. Lond; 211: 564-587, 1952.

[20]   J.E. Ffowcs Williams, D.L. Hawkings: Sound generated by turbulence and surfaces in arbitrary motion. Philosophical Transactions of the Royal Society; 264: 321–342, 1969.

[21]   F. Farassat: Linear acoustic formulas for calculation of rotating blade noise. AIAA J; 19: 1122-1130, 1981.

[22]   A.K. Singhal, M.M. Athavale, H. Li and Y. Jiang: Mathematical basis and validation of the full cavitation model. ASME Journal Fluids Eng; 124: 617-624, 2002.

[23]   S. Ivanell: Hydrodynamic simulation of a torpedo with pump jet propulsion system. Master thesis, Stockholm, 2001.

[24]   Kulczyk, J., Skraburski, L. and Zawislak, M., "Analysis of screw propeller 4119 using the Fluent system", Archives of civil and mechanical engineering, 7, No.4, pp. 129-136 (2001).

[25]   Specialist Committee on Hydrodynamic Noise, 27th International towing tank conference. Copenhagen, Denmark, Aug. 31-Sep.5, 2014.

[26]   F. Jacobsen, T. Poulsen and J.H. Rindel: Fundamentals of acoustics and noise control. Department of Electrical Engineering, Technical University of Denmark, Note no 31200, 2011.

Mohammad R Bagheri (Ph.D. Student)
Hamid Mehdigholi (Assistant Professor), mehdi@sharif.edu, +98 2166005817
Mohammad S Seif (Professor)
Center of Excellence in Hydrodynamic and Dynamic of Marine Vehicles, Department of Mechanical Engineering, Sharif University of Technology, Tehran, Iran, P.O. Box 16765-163.
Omar Yaakob (Professor)
Marine Technology Centre, Universiti Teknologi Malaysia, 81310 UTM Skudai, Malaysia.